

1 **Retrieval of aerosol optical depth from surface solar radiation measurements using machine**  
2 **learning algorithms, nonlinear regression and a radiative transfer based look-up table**

3 **J. Huttunen<sup>1,2</sup>, H. Kokkola<sup>1</sup>, T. Mielonen<sup>1</sup>, M. E. J. Mononen<sup>3</sup>, A. Lipponen<sup>1,2</sup>, J. Reunanen<sup>4</sup>, A. V.**  
4 **Lindfors<sup>1</sup>, S. Mikkonen<sup>2</sup>, K. E. J. Lehtinen<sup>1,2</sup>, N. Kouremeti<sup>5,6</sup>, A. Bais<sup>6</sup>, H. Niska<sup>7</sup> and A. Arola<sup>1</sup>**

5 [1]{Finnish Meteorological Institute (FMI), Atmospheric Research Centre of Eastern Finland, Kuopio,  
6 Finland.}

7 [2]{Department of Applied Physics, University of Eastern Finland, Kuopio, Finland.}

8 [3]{Kuopio, Finland.}

9 [4]{Tomaattinen Oy, Helsinki, Finland.}

10 [5] {Physikalisch-Meteorologisches Observatorium Davos, Dorfstrasse 33, CH-7260 Davos Dorf,  
11 Switzerland.}

12 [6] {Aristotle University of Thessaloniki, Laboratory of Atmospheric Physics, Thessaloniki, 54124,  
13 Greece.}

14 [7]{Department of Environmental and Biological Sciences, University of Eastern Finland, Kuopio,  
15 Finland.}

16 Corresponding author: J. Huttunen, Finnish Meteorological Institute (FMI), Kuopio Unit, P.O.  
17 Box 1627, FI-70211 Kuopio, Finland. (jani.huttunen@fmi.fi)

18 Key points:

19 -Machine learning methods can produce very good aerosol optical depth estimates from surface solar  
20 radiation data

21 -These tools have the potential to be used to retrieve long aerosol optical depth time series from surface  
22 solar radiation measurements

23

24 **Abstract**

25 In order to have a good estimate of the current forcing by anthropogenic aerosols knowledge on past  
26 aerosol levels is needed. Aerosol optical depth (AOD) is a good measure for aerosol loading. However,  
27 dedicated measurements of AOD are only available from 1990's onward. One option to lengthen the  
28 AOD time series beyond 1990's is to retrieve AOD from surface solar radiation (SSR) measurements  
29 done with pyranometers. In this work, we have evaluated several inversion methods designed for this  
30 task. We compared a look-up table method based on radiative transfer modelling, a nonlinear regression  
31 method and four machine learning methods (Gaussian Process, Neural Network, Random Forest and  
32 Support Vector Machine) with AOD observations done with a sun photometer at an Aerosol Robotic  
33 Network (AERONET) site in Thessaloniki, Greece. Our results show that most of the machine learning  
34 methods produce AOD estimates comparable to the look-up table and nonlinear regression methods.  
35 All of the applied methods produced AOD values that corresponded well to the AERONET  
36 observations with the lowest correlation coefficient value being 0.87 for the Random Forest method.  
37 While many of the methods tended to slightly overestimate low AODs and underestimate high AODs,  
38 Neural network and support vector machine showed overall better correspondence for the whole AOD  
39 range. The differences in producing both ends of the AOD range seem to be caused by differences in  
40 the aerosol composition. High AODs were in most cases those with high water vapour content which  
41 might affect the aerosol single scattering albedo (SSA) through uptake of water into aerosols. Our study  
42 indicates that machine learning methods benefit from the fact that they do not constrain the aerosol  
43 SSA in the retrieval where as the LUT method assumes a constant value for it. This would also mean  
44 that machine learning methods could have potential in reproducing AOD from SSR even though SSA

45 would have changed during the observation period.

46

## 47 **1.Introduction**

48 The Fifth Assessment Report of the Intergovernmental Panel on Climate Change states that the most  
49 significant source of uncertainty in the projections of climate is related to aerosols (IPCC, 2013). One  
50 significant contribution to this uncertainty comes from the fact that without the knowledge of the  
51 aerosol burden in the past, we are not able to estimate the current forcing of anthropogenic aerosol. For  
52 example, the effect of changes in the current aerosol emissions on climate depends on the background  
53 aerosol load during the pre-industrial era (e.g. Andreae, 2008; Carslaw et al., 2013). In addition, the  
54 current estimates of past aerosol emissions are highly uncertain (Granier et al., 2011) thus increased  
55 knowledge on historical aerosol levels would increase our ability to estimate the present day aerosol  
56 radiative forcing.

57 One limiting factor in determining the properties of global aerosol in the past has been that  
58 observations of aerosol radiative effects have been limited to fairly recent periods. For example, the  
59 aerosol optical depth has mainly been measured using sun photometers and the most widely known  
60 ground-based network of sun photometers is Aerosol Robotic Network (AERONET; Holben et al.,  
61 1998). Although, AERONET contains globally already over 700 stations, with a fairly good spatial  
62 coverage compared to many other observation networks, it still lacks in temporal coverage, providing  
63 aerosol optical properties and AOD only since 1990s, and reaching the current status until the recent  
64 years. The earliest records of satellite-based AOD are provided by TOMS (Total Ozone Mapping  
65 Spectrometer, e.g. Torres et al., 2002) and AVHRR (Advanced Very High Resolution Radiometer,

66 Geogdzhayev et al., 2005), from 1979 and 1983 onwards, respectively. However, neither one of these  
67 instruments were specifically designed to retrieve aerosol properties. The more recent dedicated aerosol  
68 sounders, such as ATSR (The Along Track Scanning Radiometer 2, Llewellyn-Jones and Remedios,  
69 2012), MODIS (Moderate Resolution Imaging Spectroradiometer, Levy et al., 2010), VIIRS (Visible  
70 Infrared Imaging Radiometer Suite, Jackson et al., 2013), and MISR (Multi-angle Imaging  
71 SpectroRadiometer, Kahn and Gaitley, 2015) offer data from 1995, 2000 and 2002 onwards,  
72 respectively. It is therefore apparent that neither sun-photometer nor satellite records of AOD are  
73 available for all the decades where industrialization has had a significant effect on the aerosol load.

74 There have been, however, recent studies where aerosol load has been indirectly retrieved from global  
75 surface solar radiation (SSR) or separately from direct and diffuse radiation measurements, which  
76 cover much longer time periods than sun photometer and satellite observations of AOD. Recently, Kudo  
77 et al., 2011 and Lindfors et al., 2013 used radiation measurements done with pyranometers and  
78 pyrhemometers to estimate AOD. Lindfors et al., 2013 demonstrated that AOD can be estimated by  
79 using SSR and water vapor information and a look-up table (LUT) generated with a radiative transfer  
80 code. Their method produces AOD estimates that have 2/3 of the results within  $\pm 20\%$  or  $\pm 0.05$  of  
81 collocated AERONET AODs. Because pyranometer SSR measurements have been done since 1950's  
82 over the globe, the usage of AOD estimates based on SSR measurements would enable us to construct  
83 AOD time series that go several decades back in time.

84 Since the 1990's machine learning methods have made their way to atmospheric sciences and have been  
85 used in e.g. satellite data processing, climate modeling, and weather prediction (Hsieh, 2009). Because  
86 of their ability to retrieve parameters from data that have strongly non-linear relationships, they have  
87 potential of retrieving AOD from a combination of solar radiation measurements and auxiliary data

88 such as water vapour content (WVC) and solar zenith angle (SZA), similarly to what was done by  
89 Lindfors et al. (2013) using a radiative transfer based approach. The aim the present work is to  
90 investigate how well machine learning methods are able to estimate AOD from pyranometer  
91 observations, by evaluating their performance in comparison with a radiative transfer based look-up-  
92 table approach. We chose four different methods: Neural Network (NN, McCulloch and Pitts, 1943),  
93 Random Forest (RF, Breiman, 2001), Gaussian Process (GP, Santner et al., 2013) and Support Vector  
94 Machine (SVM, Smola and Schölkopf, 2004) and compared them against a look-up table and a  
95 nonlinear regression method (NR, Bates and Watts, 1988). The performance of these methods was  
96 evaluated with AERONET AOD observations done in Thessaloniki, Greece, after the AOD estimates  
97 were derived with SSR observations. Nonlinear regression has been successfully used in multiple  
98 studies within aerosol and atmospheric sciences (e.g. Huttunen et al., 2014; Ahmad et al., 2013). Out of  
99 these machine learning methods, Neural network (NN) has been actively used in different types of  
100 applications in atmospheric sciences. For example, it has been applied to retrieve aerosol properties  
101 from remote sensing instruments (Olcese et al. 2015; Taylor et al., 2014). Moreover, Foyo-Moreno et al,  
102 2014 uses NN to indicate that a ratio between solar diffuse radiation and normal direct irradiance is the  
103 most adequate parameter to estimate AOD from solar radiation measurements. There have been,  
104 however, recent studies where aerosol load has been indirectly retrieved from global surface solar  
105 radiation (SSR) or separately from direct and diffuse radiation measurements, which cover much  
106 longer time periods than sun photometer and satellite observations of AOD. Recently, Kudo et al., 2011  
107 and Lindfors et al., 2013 used radiation measurements done with pyranometers and pyrheliometers to  
108 estimate AOD. The study by Olcese et al. 2015 is similar to ours in the sense that they use alternative  
109 data together with Neural Network approach in an attempt to retrieve AOD at an AERONET site. In  
110 their study, they fill in missing AOD values (due to e.g. cloud cover) at one AERONET station based on

111 trajectories and AOD observed on another site. To our knowledge, the rest of the analyzed methods  
112 have not been used to retrieve aerosol properties directly from observations.

## 113 **2. Data and Methods**

114 We compared the ability of several methods to estimate AOD, based on SSR and water vapor  
115 measurements (and SZA that can be readily determined for any given time and location), against  
116 AERONET AOD measurements at 500 nm (henceforth AOD) done at Thessalonki, Greece. This site  
117 was chosen for this study, because it has all the necessary measurements with high quality from a 10  
118 year time period, and because it is the same site to which Lindfors et al. (2013) applied their LUT-  
119 approach. Furthermore, the location has varying aerosol concentrations and relatively high AOD values  
120 throughout the year.

### 121 **2.1 Pyranometer measurements of surface solar radiation**

122  
123 SSR has been measured at Thessaloniki since January 1993 with a CM21 pyranometer manufactured by  
124 Kipp and Zonen. The instrument is located on the roof of the Physics Department at the Aristotle  
125 University of Thessaloniki (40.63 N, 22.96 E), ca. 60 m above sea level. The data are sampled every 1–  
126 2 s and every minute the average and standard deviation of the samples are recorded (see more details  
127 from Lindfors et al., 2013). The calibration of the pyranometer has been confirmed to stay within the  
128 quoted by the manufacturer accuracy (Bais et al., 2013).

### 129 **2.2 AERONET measurements**

130 AERONET is a network of sun and sky scanning radiometers that measure direct sun and sky radiance  
131 at several wavelengths, typically centered at 340, 380, 440, 500, 670, 870, 940, and 1020 nm, providing

132 measurements of various aerosol related properties (Holben et al., 1998). From direct sun  
133 measurements we exploited AOD and WVC data. When also sky radiance measurements are included,  
134 more detailed aerosol properties such as single scattering albedo (SSA) and asymmetry parameter (gg)  
135 can be retrieved (Dubovik et al., 2000). In the evaluation of the machine learning methods we used  
136 Level 2.0 (cloud-screened and quality assured) AERONET direct sun measurements of AOD and WVC  
137 for Thessaloniki. The Cimel sun photometer is located at the roof of the Physics Department in the  
138 close vicinity of the pyranometer discussed above. From the inversion products, to interpret some of our  
139 results in more detail, we used level 1.5 (cloud-screened) retrievals. However, when we selected the data  
140 from the Level 1.5 inversion product, we applied all the other level 2.0 AERONET criteria except for  
141 the AOD threshold. In other words, we applied otherwise the same rigorous quality control that is  
142 required for Level 2 data, but we only relaxed the requirement for AOD at 440nm to range from 0.4 to  
143 0.1, in order to have more reliable measurements for our data analysis.

### 144 **2.3 Cloud-screening of the pyranometer measurements and collocation with the AERONET** 145 **measurements**

146 Cloud-screening is a crucial factor in the analysis, thus only contribution of aerosols are considered, not  
147 clouds. The SSR data was at first cloud-screened in order to ensure that only clear-sky measurements  
148 were included in the analysis (see Lindfors et al., 2013 for more details). However, during the analysis  
149 of the data it became evident that even after the initial cloud-screening, the SSR data still included  
150 observations that deviated significantly from the main body of the observations. Since there is a high  
151 probability that these outliers in the data were caused by e.g. cloud-contamination, we applied  
152 additional screening to the data. Thus, we removed the clear outliers of possibly undetected clouds, in  
153 our case those observations that deviated by more than  $\pm 20 \text{ Wm}^{-2}$  from the exponential regression fit

154 (SSR =  $a \times \exp(-b \times \text{AOD}) + c$ , where a, b and c are regression constants). This additional screening was  
155 applied through regression of SSR against AOD for a given range of SZA (within  $\pm 0.5^\circ$ ). It has to be  
156 noted that this data was only a small fraction of all the data that remained after the cloud screening and  
157 it is very unlikely that the additional cloud-screening would affect the main results and the conclusions  
158 of our study.

159 The SSR values were collocated for each AOD with the  $\pm 1$  minutes difference, averaged and finally  
160 normalized for the Sun-Earth distance corresponding to January 1<sup>st</sup>. The training dataset for the  
161 machine learning methods contained years 2009-2014 and the validation (verification) dataset years  
162 2005-2008. These periods were selected because we wanted to verify if the methods could provide  
163 reasonable AOD estimates for a period different than the training. The training dataset covered  
164 approximately 2/3 and the validation dataset 1/3 of the whole data. For all the methods the input  
165 parameters are SSR, WVC and SZA, and they produce AOD estimates (Table A1 summarises the  
166 statistics of maximum, minimum, average, STD and median for the input and the output parameters.  
167 Table A1 shows that e.g. AOD is larger for the validation dataset, although the maximum value is larger  
168 for the training).

169

## 170 **2.4 LUT and NR methods for AOD retrievals**

171

### 172 **2.4.1 Radiative transfer model based look-up table (LUT)**

173 To retrieve AOD from SSR observations Lindfors et al., (2013) produced a LUT based on radiative  
174 transfer simulations. They simulated SSR in different atmospheric conditions by varying AOD, WVC



175 and SZA systematically. They used a single aerosol model for all the simulations, and therefore called  
 176 their AOD estimate as an effective AOD, which is only a function of SSR, SZA, WVC. Other  
 177 parameters were assumed as constants e.g. Ångström Exponent of 1.1, SSA at 500 nm of 0.92 (the  
 178 SSA's spectral pattern follows the rural background aerosol model by Shettle, 1989, where SSA changes  
 179 from roughly 0.92 at 400 nm to 0.89 at 1000 nm), the asymmetry parameter was assumed wavelength  
 180 independent with a value of 0.68 while the albedo was varying with wavelength and SZA. For a more  
 181 detailed description of the LUT method see Lindfors et al., (2013).

#### 182 **2.4.2 Nonlinear regression method (NR)**

183 The nonlinear regression (NR) is a multivariate analysis method which is used when the dependencies  
 184 between the study variables are not linear (Bates and Watts, 1988). NR is useful especially when there  
 185 are physical reasons for believing that the relationship between the response and the predictors follows a  
 186 particular functional form. Benefits of NR are that it needs only moderate sized sample of the studied  
 187 phenomena to give adequately precise results and as an output it gives a simple, but not predefined,  
 188 function for prediction. Additional advantage of NR against the other methods presented in this paper is  
 189 that once the parameters are estimated, they can be used in similar cases without additional training  
 190 data. In this study we assume that AOD can be estimated as a function of SSR, WVC and SZA.  
 191 Multiple different formulations for the NR function was tested and the function with the best prediction  
 192 ability found for this data is given by

$$\begin{aligned}
 \text{AOD} = & b_0 + b_1 \exp\left(\frac{1}{\text{SZA}}\right) + b_2 \exp\left(\frac{1}{\text{SSR}}\right) + b_3 \exp\left(\frac{1}{\text{WVC}}\right) \\
 & + b_4 \exp\left(\frac{1}{\text{SZA}} + \frac{1}{\text{SSR}}\right) + b_5 \exp\left(\frac{1}{\text{SZA}} + \frac{1}{\text{WVC}}\right) + b_6 \exp\left(\frac{1}{\text{SSR}} + \frac{1}{\text{WVC}}\right). \quad (1)
 \end{aligned}$$

193

194 The coefficients  $b_0$ - $b_6$  were determined using R-software (R Core Team, 2014) and are shown in Table  
195 A2.

## 196 **2.5 Machine learning methods for AOD retrievals**

197

### 198 **2.5.1 Neural Network (NN)**

199 Artificial neural networks belong to the family of machine learning methods (McCulloch and Pitts,  
200 1943). As usual in machine learning methods, the aim of an artificial NN is to generate a mathematical  
201 model to represent the phenomenon that is examined. The mathematical model of NN structure  
202 specifically consists of interconnected neurons with numeric weights. A typical NN model is multilayer  
203 perceptron (MLP) (Rosenblatt, 1958), which is used in this study. A MLP network consists of several  
204 neuron layers: an input layer, hidden layers and an output layer. The weights and other parameters of the  
205 model are tuned or trained with a specific training data set containing input-output pairs of the  
206 phenomenon. In this case the model inputs are SSR, WVC, SZA and the output is AOD. The training is  
207 executed with a training algorithm and in this paper the Levenberg-Marquardt algorithm is used (Hagan  
208 and Menhaj, 1994). A total of 20 NNs were trained in this case. The NNs differed from each other by  
209 the number of neurons in a hidden layer. Five networks with the smallest prediction error within the  
210 training data set were selected to the final committee of networks. The final prediction of the NN model  
211 was computed as a median of the outputs of all networks in the committee. For more information on  
212 NNs see, for example, Bishop, (1995).

### 213 **2.5.2 Random Forest (RF)**

214 Random Forest is a machine learning technique that may be used for classification and nonlinear  
215 regression (Breiman, 2001). RF for nonlinear regression consists of an ensemble of binary regression

216 trees. Each of these trees is constructed using a randomized training scheme and is essentially a  
217 piecewise constant fit to the training data set. The prediction of a RF model is obtained by averaging  
218 the regression tree predictions over the whole model ensemble. In this study, the RF implementation  
219 from the Scikit-Learn machine learning library (Pedregosa et al. 2011) was used. We used (SSR, WVC,  
220 SZA, SSRxWVC, SSWxSZA, WVCxSZA) as the RF model inputs and AOD as the output. A  
221 randomized cross-validation scheme was used to find the optimal training parameters for the RF. For  
222 more information on RFs see, for example, Friedman et al., (2001).

### 223 **2.5.3 Support vector machine (SVM)**

224 Support vector machine (SVM) is a machine learning technique (Vapnik, 1995; Burges, 1998). In this  
225 study, we use the standard SVM regression (SVR), the formulation based on the commonly used  $\epsilon$ -SVR  
226 with radial basis kernel function. For implementing the SVM the libsvm package was used (Chang and  
227 Lin, 2011). The objective of  $\epsilon$ -SVR is to find a function that has at most  $\epsilon$  deviation from the training  
228 data set outputs. The training of an  $\epsilon$ -SVR model is formulated as a quadratic (convex) optimization  
229 problem in which the Vapnik's  $\epsilon$ -insensitive loss function is minimized (e.g. Vapnik 1995). The  $\epsilon$ -SVR  
230 model has two training parameters that were used to control the training: the regularization parameter,  
231 which controls the smoothness of the approximation function (sensitivity to noise), and the parameter  
232  $\epsilon$ , which dominates the number of support vectors by governing the accuracy of the approximation  
233 function. The determination of SVM control parameters was solved by the means of a grid search. For a  
234 more detailed description of the method, the reader is referred, for example, to Smola and Schölkopf  
235 (2004).

### 236 **2.5.4 Gaussian process (GP)**

237 Gaussian process (GP) for machine learning is a generic supervised learning method that may be used,  
238 for example, for nonlinear regression. In GP learning, the function inputs and outputs are treated as  
239 Gaussian random variables and the correlations between these variables are modelled. The predictions  
240 given by a GP model are computed as conditional probability distributions given the training data and  
241 function inputs. As the prediction given by a GP model is a probability distribution, the error estimates  
242 for the predicted point estimates are obtained automatically. In this study, the GP implementation from  
243 the Scikit-Learn machine learning library was used. The same inputs and output variables as with the  
244 RF models were used in the GP training. The best performing correlation function training parameters  
245 were sought for using maximum likelihood estimation. A total of 25 GP models were trained. The  
246 training of each model was carried out using 2500 training data samples that were randomly sampled  
247 from the full training data set. The five best performing GP models were selected into the final GP  
248 model committee. The final prediction was computed as the median of the predictions given by the GP  
249 models in the committee. For more information on GPs for machine learning see, for example, Welch et  
250 al., (1992), Rasmussen and Williams (2006), and Santner et al., (2013).

## 251 **3. Results**

### 252 **3.1 Comparison of the methods**

253 Table 1 shows the statistics of the AOD observed by AERONET together with the statistical  
254 characteristics of the predicted AOD for the years 2005-2008. From the table, we can see that predicted  
255 values show good correlation against the observations for all the methods. Predictions by RF had the  
256 lowest correlation coefficient with a value of 0.87 while the correlation coefficient for NR was only  
257 slightly larger, 0.88. For the best performing methods, LUT, GP, NN, and SVM, the correlation

258 coefficients were approximately 0.92. Their predicted AODs in comparison to AERONET AOD are  
259 shown in Figure 1. To visualize the distribution of the data, the colorbar in Figure 1 represents the  
260 number of observations for each AOD interval of 0.005. Based on the different statistics in Table 1,  
261 machine learning methods (NN, SVM, GP) produce a good match with AERONET data and they  
262 perform equally good or better than the LUT method according to all the metrics. Due to the fact that  
263 RF and NR are not able to produce as good estimates as the LUT method, they were left out from the  
264 more detailed analysis.

265 Although these methods are able to predict the average AOD with a good accuracy, they differ when we  
266 compare their ability to predict different AOD levels. In Figure 1, the color scales indicate the absolute  
267 amount of results in the areas with the interval of  $0.01 \times 0.01$  (vertically and horizontally) for AOD, in  
268 addition 1:1-lines and linear fits are included. Based on the linear fits, NN appears to have the best  
269 agreement with AERONET data for the whole AOD range. As the average and median values of  
270 AERONET AOD are 0.240 and 0.207 respectively (Table 1), the main population of the measurements  
271 is in the range of moderate AODs. The machine learning methods are obviously weighted to perform  
272 best in this range of AODs. However, from Figure 2, which shows the absolute difference between  
273 AERONET and predicted AOD, we can see that LUT and GP tend to significantly underestimate AOD  
274 for AODs larger than 0.5, while NN and SVM are able to reach smaller differences with AERONET on  
275 average, although with larger overall variabilities than LUT and GP. Although NN and SVM also start  
276 to deviate from the observations at higher AODs, these deviations are more modest in relative sense as  
277 can be seen from Figure 3 which shows the relative difference between the observations and  
278 predictions. All the methods overestimate AOD in relative terms, when AOD approaches zero (Figure  
279 3). However, as Figure 2 demonstrates, the absolute error is systematically very low in the small AOD

280 region ( $AOD < 0.2$ ). NN and SVM are generalized better for large AODs than the other methods, where  
281 the amount of data are small.

282 As an additional test, we tested combining different the colorbar in Figure 1 represents the number of  
283 observations for each AOD interval of 0.005. methods. In Table 1, the four last rows represent the  
284 values for cases where the results of machine learning methods are combined by averaging them. As  
285 can be seen from the table, these combinations do not improve the estimates compared to the statistical  
286 values of individual methods.

### 287 **3.2 The effect of water vapour on AOD predictions**

288 Huttunen et al. (2014) showed that WVC and AOD have typically a positive correlation. Therefore, we  
289 investigated how the AOD estimates from different methods are affected by WVC. Figure 4 shows the  
290 relative difference between the predictions and measured AOD with respect to WVC. From this figure,  
291 we can see that the LUT-based AODs are overestimated at the smallest and underestimated at the largest  
292 WVC contents. The reason for this behaviour is that the LUT method has been set to assume prescribed  
293 and constant properties for many relevant parameters that affect SSR (other than AOD and WVC); e.g.  
294 aerosol single scattering albedo, asymmetry parameter and surface albedo (Lindfors et al., 2013).  
295 Consequently, the assumption of constant SSA in particular leads to WVC-dependent systematic bias of  
296 the LUT-based AOD, as we will show next. The other methods are closer to the ratio of 1 without such  
297 a systematic bias, excluding the SVM's underestimation for the smallest WVC.

298 Figure 5 shows measured SSR and LUT-based SSR for a narrow set of SZAs ( $48.50^\circ$ - $51.50^\circ$ ). AOD is  
299 on the horizontal axis, SSR on the vertical axis and WVC is shown with the colorbar. From Figure 5a it  
300 is evident that LUT incorporates a strong WVC-dependent structure: for a given SSR level, AOD

301 decreases with increasing water vapor content. This pattern follows from the assumption that the  
302 aerosol composition remains the same, i.e. it has a fixed SSA value. Thus in the LUT method, increases  
303 in SSR absorption by water vapour are compensated by decreases in aerosol extinction. In the real  
304 atmosphere, water vapour content has also implications on aerosol composition and size. If all  
305 conditions apart from water vapour remained constant, increase of water vapour would also increase the  
306 uptake of water into aerosol particles thus affecting the aerosol SSA. The effect of fixed SSA is also  
307 visible in the way the LUT-based AOD estimates are distributed (Figure 5a). In Figure 5c we can see  
308 that for a given AOD in the LUT, the highest WVC values always correspond to the lowest SSR values.  
309 However, the same pattern is not clearly visible either in the plot with the measured values (Figure 5b)  
310 or in the plot with AOD from NN (Figure 5d). This indicates that although the machine learning  
311 methods do not get explicitly any information about the possible systematic co-variability of WVC and  
312 SSA, they seem to be able to detect it indirectly, at least to some extent.

313 To further illustrate this, Figure 6a shows the AERONET measurements of AOD and single scattering  
314 co-albedo,  $1-SSA$  at 500 nm as a function of WVC. Here, together with the absorption strength by the  
315 water vapour, we considered more illustrative to show the single scattering co-albedo rather than SSA.  
316 In this plot, SZA, SSR and season were limited respectively to:  $58^\circ < SZA < 62^\circ$ ,  $420 \text{ Wm}^{-2} < SSR <$   
317  $460 \text{ Wm}^{-2}$ , June-August, allowing enough data with the limited parameters. Thus, the plot illustrates the  
318 co-variability of WVC and SSA for a limited range of surface solar radiation and SZA, for conditions  
319 when the LUT method produces lower AOD values for higher WVC (Figure 5a). However, Figure 6a  
320 clearly shows that an opposite relationship between AOD and WVC is obtained by the measurements.  
321 Moreover, this pattern is compensated by aerosol absorption (remember that in this sub-set we  
322 constrained SSR), which decreases with increasing WVC; this is likely related to the aerosol swelling

323 by hygroscopic growth that increases the scattering of the aerosol. Therefore, we can conclude from the  
324 measurements that because of the co-variability of WVC and SSA in Thessaloniki, the assumption of a  
325 fixed SSA in the LUT causes limitations for predicting AOD, while the machine learning methods can  
326 take into account, at least to some extent, this relationship indirectly. Using radiative transfer modeling  
327 we demonstrated that the magnitude of these changes in water vapor and aerosol absorption, as  
328 indicated in Figure 6. Indeed, they induced opposite effects of similar magnitude in surface solar  
329 irradiance. For the base case, we simulated SSR with WVC of 2.8 cm and 1-SSA of 0.06 (with SZA of  
330  $60^\circ$  and AOD of 0.3) as inputs, resulting in  $439.9 \text{ Wm}^{-2}$ . When we increased the water vapour column  
331 to 3.6 cm, the corresponding decrease in SSR was about  $6.8 \text{ Wm}^{-2}$ . However, when we additionally  
332 decreased the aerosol absorption (1-SSA) to 0.04, the difference to the base case shrank to  $1.8 \text{ Wm}^{-2}$   
333 and this remaining amount can mostly be explained by the asymmetry parameter, which also exhibits a  
334 systematic dependence with WVC (stronger forward scattering by particles grown in humid conditions).

335 The lower panel of Figure 6 further illustrates the role of fixed SSA in the observed WVC-dependent  
336 bias in the LUT results, which can be avoided with the machine learning methods. It shows the mean  
337 ratio of LUT-estimated and AERONET-measured AOD on the right-hand side y-axis as a function of  
338 water vapour content (so essentially the same results shown by a box-plot in Figure 4). Additionally, on  
339 the left-hand side y-axis, the single scattering albedo (estimated for 500 nm) from AERONET  
340 measurements is shown as a function of water vapour amount as well. This also demonstrates that the  
341 over- and underestimations of the LUT method coincide with SSA range that is under and over the  
342 assumed fixed value of 0.92 (shown with red dashed line), respectively. Visibly, the ratio in the right-  
343 hand axis of Fig. 6b, reaches one not until SSA is roughly 0.93 instead of 0.92. Presumably, SSA has  
344 actually a different wavelength pattern than the one assumed in LUT.



#### 345 **4. Conclusions**

346 We have used several inverse methods to retrieve aerosol optical depth (AOD) from surface solar  
347 radiation (SSR) and water vapour content (WVC) measurements (with corresponding solar zenith angle  
348 data) done in Thessaloniki, Greece. Two traditional (look-up table (LUT) and nonlinear regression  
349 (NR)) and four machine learning methods (Gaussian Process (GP), Neural Network (NN), Random  
350 Forest (RF) and Support Vector Machine (SVM)) were used to retrieve AOD estimates for the years  
351 2005-2008. Then we compared the AOD estimates with collocated AOD measurements done by  
352 Aerosol Robotic Network (AERONET). Our comparisons showed that:

353 -AOD estimates based on the LUT method agreed better with AERONET than the NR estimates but  
354 apart from RF, the machine learning methods produced AOD estimates that were comparable or better  
355 than LUT.

356 -NN and SVM methods reproduced good correspondence to AERONET observations for both low and  
357 high AODs while rest of the methods tended to overestimate low AODs and underestimate high AODs.

358 The main reason for the better performance of these machine learning methods was that there were no  
359 constraints of the aerosol single scattering albedo (SSA) in the retrieval. In other words, the methods do  
360 not need to explicitly make assumptions on the optical aerosol properties of the atmosphere and  
361 because seem to be able to indirectly account for the covariation of WVC and SSA.

362 -When compared with AERONET measurements, the best AOD estimates were retrieved with the  
363 machine learning algorithms, but only NN and SVM were able to generalize accurate estimates also for  
364 large AODs.

365 -The machine learning methods are sensitive to the selection of the training data set and other

366 constraints, and are generally valid only for the range of the variables used for their training; thus care  
367 needs to be taken when these methods are employed.

368 -These tools have the potential to be used in the retrieval of AOD from SSR measurements to lengthen  
369 the time series of AOD. Historical AOD is essential in the estimation of anthropogenic aerosol effects  
370 and in the evaluation of AOD retrievals from space borne instruments before the 1990s.

371 -The intention of comparing different methods was to test their ability in an "out-of-the-box"  
372 configuration. With this in mind, methods were not particularly tuned to reach the best possible results.  
373 It is very likely that e.g. optimizing the free parameters used in each of the nonlinear modeling  
374 approaches, their ability to reproduce observed AOD could be further improved.

### 375 **Acknowledgements.**

376 We thank the AERONET team, principal investigators and other participants for their effort in  
377 establishing and maintaining the network. This study is supported by Graduate school in Physics,  
378 Chemistry, Biology and Meteorology of Atmospheric Composition and Climate Change: From  
379 Molecular Processes to Global Observations and Models. The Academy of Finland Center of  
380 Excellence program (project number 272041) is also acknowledged. The financial support by the  
381 strategic funding of the University of Eastern Finland is gratefully acknowledged. The author thank  
382 Juha Tonttila and Mikko Pitkänen from Finnish Meteorological Institute, Kuopio, for their help with the  
383 python (python.org) and in the production of the MatLab (mathworks.com) boxplot-figures. Also JH  
384 thank the Finnish Cultural Foundation, North Savo Regional fund.

### 385 **References**

386 Ahmad, I., Mielonen, T., Grosvenor, D., Portin, H., Arola, A., Mikkonen, S., Kühn, T., Leskinen, A.,  
387 Joutsensaari, J., Komppula, M., Lehtinen, K., Laaksonen, A. and Romakkaniemi, S. (2013). Long-term  
388 measurements of cloud droplet concentrations and aerosol-cloud interactions in continental boundary

389 layer clouds. *Tellus B*, 65. doi:<http://dx.doi.org/10.3402/tellusb.v65i0.20138>.

390 Andreae, M. O. and Rosenfeld, D. Aerosol–cloud–precipitation interactions. Part 1. The nature and  
391 sources of cloud-active aerosols, *Earth Sci. Rev.* 89, 13–41, 2008.

392 Bais, A. F., Drosoglou, Th., Meleti, C., Tourpali, K. and Kouremeti, N., Changes in surface shortwave  
393 solar irradiance from 1993 to 2011 at Thessaloniki (Greece). *Int. J. Climatol.*, 33: 2871–2876. doi:  
394 10.1002/joc.3636, 2013.

395 Bates D.M. and Watts D. G., *Nonlinear Regression Analysis and Its Applications*, Wiley, New York,  
396 1988.

397 Bishop C. M., *Neural Networks for Pattern Recognition*, Oxford University Press, Inc. New York, NY,  
398 USA, ISBN:0198538642, 1995.

399 Breiman, L., Random forests, *Machine learning*, vol 45, 1, 5-32, 2001.

400 Burges C. J. C., A tutorial on support vector machines for pattern recognition, *Data Mining and*  
401 *Knowledge Discovery*, 2, 121–167, 1998.

402 Carslaw K. S., Lee L. A., Reddington C. L., Pringle K. J., Rap A., Forster P. M., Mann G. W.,  
403 Spracklen D. V., Woodhouse M. T., Regayre L. A. and Pierce J. R., Large contribution of natural  
404 aerosols to uncertainty in indirect forcing, *Nature*, 2013.

405 Dubovik, O., A. Smirnov, B. N. Holben, M. D. King, Y.J. Kaufman, T. F. Eck, and I. Slutsker, 2000:  
406 Accuracy assessments of aerosol optical properties retrieved from AERONET sun and sky-radiance  
407 measurements, *J. Geophys. Res.*, 105, 9791-9806.

408 Foyo-Moreno I., Alados I., Anton M., Fernandez-Galvez J., Cazorla A. and Alados-Arbodelas L.,  
409 Estimating aerosol characteristics from solar irradiance measurements at an urban location in  
410 southeastern Spain, *J. of Geophys. Res. Atmos*, 119, 1845-1859, doi:10.1002/2013JD020599, 2014.

411 Friedman J., Hastie T., and Tibshirani R., *The elements of statistical learning*, Springer, vol 1, 2001.

412 Geogdzhayev, I. V., M. I. Mishchenko, E. I. Terez, G. A. Terez, and G. K. Gushchin, Regional advanced  
413 very high resolution radiometer–derived climatology of aerosol optical thickness and size, *J. Geophys.*  
414 *Res.*, 110, D23205, doi:10.1029/2005JD006170, 2005.

415 Chang C.-C. and Lin C.-J. LIBSVM: a library for support vector machines. *ACM Transactions on*  
416 *Intelligent Systems and Technology*, 2:27:1-27:27, 2011.

417 Claire Granier, Bertrand Bessagnet, Tami Bond, Ariela D’Angiola, Hugo Denier van der Gon, Gregory  
418 J. Frost, Angelika Heil, Johannes W. Kaiser, Stefan Kinne, Zbigniew Klimont, Silvia Kloster, Jean-  
419 François Lamarque, Catherine Lioussse, Toshihiko Masui, Frederik Meleux, Aude Mieville, Toshimasa  
420 Ohara, Jean-Christophe Raut, Keywan Riahi, Martin G. Schultz, Steven J. Smith, Allison Thompson,  
421 John van Aardenne, Guido R. van der Werf, and Detlef P. van Vuuren, Evolution of anthropogenic and  
422 biomass burning emissions of air pollutants at global and regional scales during the 1980–2010 period,  
423 *Climatic Change*, 109, 1, 163-190, 2011.

424 Hagan M.T. and Menhaj M.B., Training feedforward networks with the Marquardt algorithm, *IEEE*  
425 *Trans. Neural Networks*, 5, 6, 989-993, 1994.

426 Holben B.N., T.F. Eck, I. Slutsker, D. Tanre, J.P. Buis, A. Setzer, E. Vermote, J.A. Reagan, Y. Kaufman,

427 T. Nakajima, F. Lavenu, I. Jankowiak, and A. Smirnov, 1998: AERONET - A federated instrument  
428 network and data archive for aerosol characterization, *Rem. Sens. Environ.*, 66, 1-16.

429 Hsieh, *Machine Learning Methods in the Environmental Sciences Neural Networks and Kernels*,  
430 Cambridge Univ Press, 2009.

431 Huttunen, J., Arola, A., Myhre, G., Lindfors, A. V., Mielonen, T., Mikkonen, S., Schafer, J. S., Tripathi,  
432 S. N., Wild, M., Komppula, M., and Lehtinen, K. E. J.: Effect of water vapor on the determination of  
433 aerosol direct radiative effect based on the AERONET fluxes, *Atmos. Chem. Phys.*, 14, 6103-6110,  
434 doi:10.5194/acp-14-6103-2014, 2014.

435 IPCC, *Climate Change 2013: The Physical Science Basis. Contribution of Working Group I to the Fifth*  
436 *Assessment Report of Intergovernmental Panel on Climate Change*, Cambridge University Press,  
437 Cambridge, United Kingdom and New York, NY, USA, ISBN 978-1-107-66182-0,  
438 doi:10.1017/CBO9781107415324, 2013.

439 Jackson, J. M., H. Liu, I. Laszlo, S. Kondragunta, L. A. Remer, J. Huang, and H.-C. Huang, Suomi-  
440 NPP VIIRS aerosol algorithms and data products, *J. Geophys. Res. Atmos.*, 118, 12, 673–12, 689,  
441 doi:[10.1002/2013JD020449](https://doi.org/10.1002/2013JD020449), 2013.

442 Kahn, R. A., and B. J. Gaitley, An analysis of global aerosol type as retrieved by MISR. *J. Geophys.*  
443 *Res. Atmos.*, 120, 4248–4281. doi: [10.1002/2015JD023322](https://doi.org/10.1002/2015JD023322), 2015.

444 Kudo, R., Uchiyama, A., Yamazaki, A., Sakami, T., and Ijima, O., Decadal changes in aerosol optical  
445 thickness and single scattering albedo estimated from ground-based broadband radiometers: A case  
446 study in Japan, *J. Geophys. Res.*, 116, D03207, doi:10.1029/2010JD014911, 2011.

447 Levy, R. C., Remer, L. A., Kleidman, R. G., Mattoo, S., Ichoku, C., Kahn, R., and Eck, T.F., Global  
448 evaluation of the Collection 5 MODIS dark-target aerosol products over land, *Atmos. Chem. Phys.*, 10,  
449 10399-10420, doi:10.5194/acp-10-10399-2010, 2010.

450 Llewellyn-Jones D. and Remedios J., The Advanced Along Track Scanning Radiometer (AATSR) and  
451 its predecessors ATSR-1 and ATSR-2: An introduction to the special issue, *Remote Sensing of*  
452 *Environment*, Vol 116, 15, Pages 1–3, doi:10.1016/j.rse.2011.06.002, 2012.

453 Lindfors, A. V., Kouremeti, N., Arola, A., Kazadzis, S., Bais, A. F., and Laaksonen, A., Effective  
454 aerosol optical depth from pyranometer measurements of surface solar radiation (global radiation) at  
455 Thessaloniki, Greece, *Atmos. Chem. Phys.*, 13, 3733-3741, doi:10.5194/acp-13-3733-2013, 2013.

456 McCulloch, W. and Pitts W., A Logical Calculus of Ideas Immanent in Nervous Activity, *Bulletin of*  
457 *Mathematical Biophysics* 5, 4, 115–133. doi:10.1007/BF02478259, 1943.

458 Olcese L. E., Palancar G. G. and Toselli B. M., A method to estimate missing AERONET AOD values  
459 based on artificial neural networks, *Atmospheric Environment*, 113, 140–150,  
460 doi:10.1016/j.atmosenv.2015.05.009, 2015.

461 Pedregosa, F., Varoquaux, G., Gramfort, A., Michel, V., Thirion, B., Grisel, O., Blondel, M.,  
462 Prettenhofer, P., Weiss, R., Dubourg, V., Vanderplas, J., Passos, A., Cournapeau, D., Brucher, M.,  
463 Perrot, M., and Duchesnay, E., Scikit-learn: Machine Learning in Python, *Journal of Machine Learning*  
464 *Research*, 12, 2825-2830, 2011.

465 R Core Team (2014). R: A language and environment for statistical computing. R Foundation for

466 Statistical Computing, Vienna, Austria. URL <http://www.R-project.org/>.

467 Rasmussen, C.E. and Williams, C.K.I., Gaussian processes for machine learning, MIT Press, 2006.

468 Santner, T. J., Williams, B. J., and Notz, W. I., The design and analysis of computer experiments,  
469 Springer Science & Business Media, 2013.

470 Rosenblatt, F. A, probabilistic model for information storage and organization in the brain, Psychol.  
471 Rev., 65, 6, 368-408, 1958.

472 Shettle, E. P., Models of aerosols, clouds and precipitation for atmospheric propagation studies, in:  
473 Atmospheric Propagation in the UV, Visible, IR and mm-region and Related System Aspects, no. 454  
474 in AGARD Conf. Proc., 15-1-15-13, 1989.

475 Smola A. J. and Schölkopf B., A tutorial on support vector regression, Stat. Comput., 14, 199-222,  
476 2004.

477 Taylor, M., Kazadzis, S., Tsekeri, A., Gkikas, A., and Amiridis, V., Satellite retrieval of aerosol  
478 microphysical and optical parameters using neural networks: a new methodology applied to the Sahara  
479 desert dust peak, Atmos. Meas. Tech., 7, 3151-3175, doi:10.5194/amt-7-3151-2014, 2014.

480 Torres, O., Bhartia P. K., Herman J. R., Sinyuk A., Ginoux P., and Holben B., A long-term record of  
481 aerosol optical depth from TOMS observations and comparison to AERONET measurements, Journal  
482 of the Atmospheric Sciences, 59, 3, 398-413, 2002.

483 Vapnik, V., The Nature of Statistical Learning Theory. New York: Springer, 1995.

484 Welch, W. J., Buck, R. J., Sacks, J., Wynn, H. P., Mitchell, T. J., and Morris, M. D., Screening,  
485 predicting, and computer experiments, Technometrics, vol 34, 1, 15-25, 1992.

486

488

489 Table 1: Statistical characteristics of observed (AERONET) and predicted AOD by the methods of NR  
490 (nonlinear regression), LUT (look-up table), NN (neural network), RF (random forest), GP (gaussian  
491 process), SVM (support vector machine) and some of their combinations (averages without weights,  
492 e.g. NN, SVM combination is their average result). Correlation coefficient ( $R^2$ ), mean absolute  
493 deviation (MAD), median and their  $\pm 20\%$  percentiles between the observed and predicted. Also time  
494 consumptions with a recent average computer power of the methods for training / estimation in the  
495 magnitude of seconds, minutes and hours. The number of observations is 10684.

Method	Average(std)	$R^2$	MAD	Median	Fraction in +/-20%	Time consumption
AERONET	<b>0.240(0.147)</b>			<b>0.207</b>		

NR	0.228(0.123)	0.880	0.053	0.210	48.4 %	seconds / < second
LUT	0.254(0.136)	0.920	0.046	0.236	52.6 %	hours / minutes
NN	0.251(0.156)	0.920	0.044	0.212	59.1 %	hours / < second
RF	0.225(0.116)	0.870	0.052	0.204	52.9 %	tens of seconds / < second
GP	0.240(0.130)	0.927	0.041	0.213	60.8 %	minutes / tens of seconds
SVM	0.242(0.150)	0.918	0.044	0.201	58.4 %	tens of seconds / < second
NN, SVM	0.247(0.152)	0.924	0.043	0.207	59.7 %	
NN, SVM, RF	0.240(0.138)	0.922	0.042	0.205	59.9 %	
SVM, RF	0.234(0.131)	0.913	0.044	0.202	58.0 %	
NN, RF	0.238(0.134)	0.916	0.043	0.207	59.0 %	

496

497

498

499

500

501

502

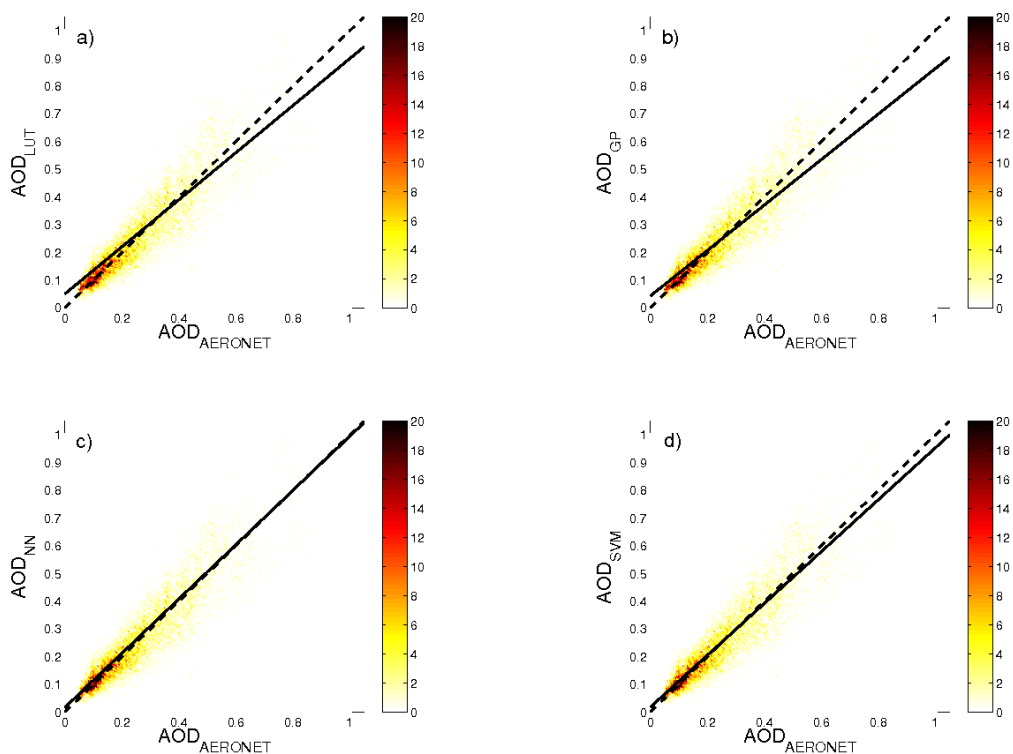
503

504

505

506

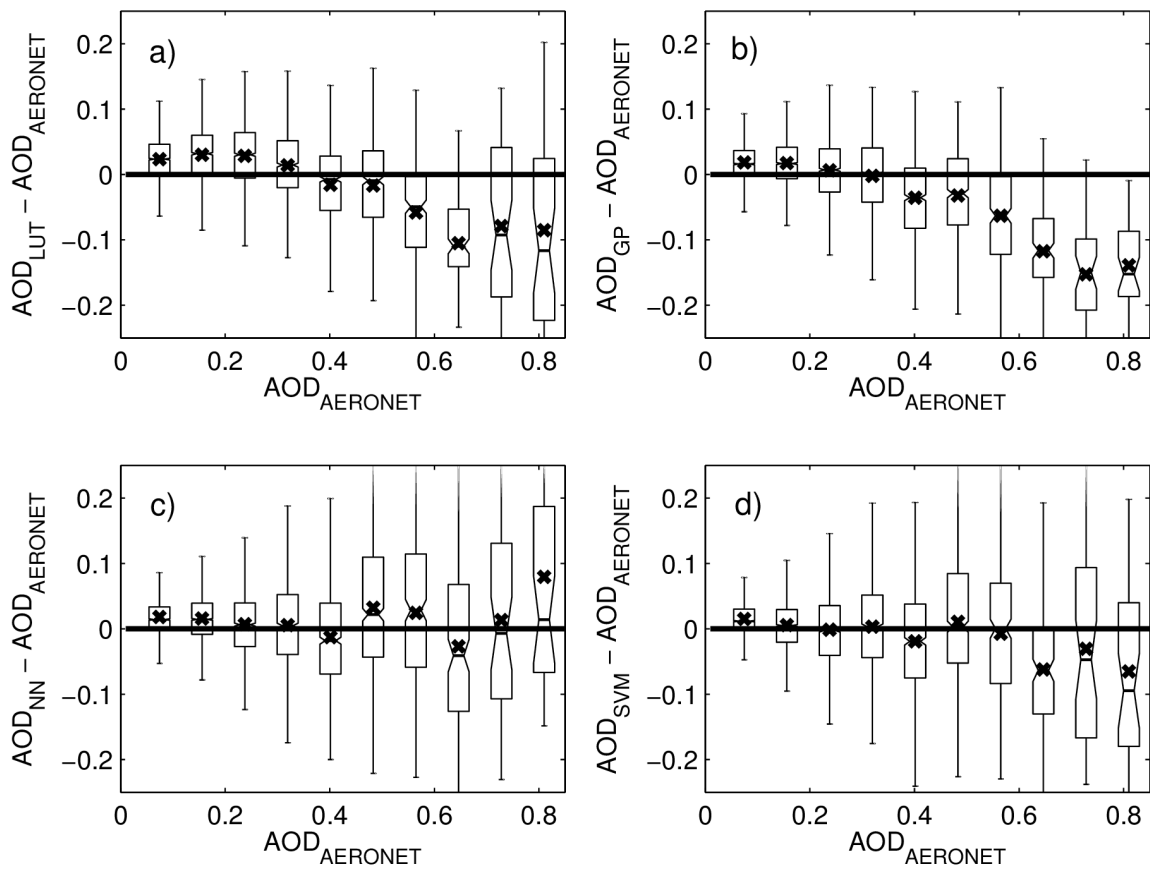
507



510 Figure 1: Observed (AERONET) and predicted AOD by the methods of a) LUT (look-up table), b) GP  
 511 (Gaussian Process), c) NN (Neural Network) and d) SVM (Support Vector Machine). The colorbar  
 512 indicates the absolute amount of results in the areas with the interval of  $0.01 \times 0.01$ . The 1:1-lines and  
 513 linear fits included. The number of observations is 10684. The relation for the linear fits is, estimated  
 514  $AOD = a_1 + a_2 \times AERONET \text{ AOD}$ , and the coefficients of the least square fits with their errors are ( $a_1$ ,  
 515  $a_2$ ):  $0.050(\pm 0.001)$ ,  $0.849(\pm 0.004)$ ;  $0.043(\pm 0.001)$ ,  $0.820(\pm 0.003)$ ;  $0.016(\pm 0.001)$ ,  $0.979(\pm 0.004)$   
 516 and  $0.018(\pm 0.001)$ ,  $0.936(\pm 0.004)$ , for LUT; GP; NN and SVM, respectively.

517

518



520 Figure 2: Differences between predicted and observed (AERONET) AOD for the methods: a) LUT  
 521 (look-up table), b) GP (Gaussian Process), c) NN (Neural Network) and d) SVM (Support Vector  
 522 Machine) with respect of the observed AOD. The crosses indicate the means of each sub-group, the  
 523 limits of the boxes are 25 %, 50 % and 75 % of the data, and the lines are plotted with 1.5 times the  
 524 inter-quartile ranges.

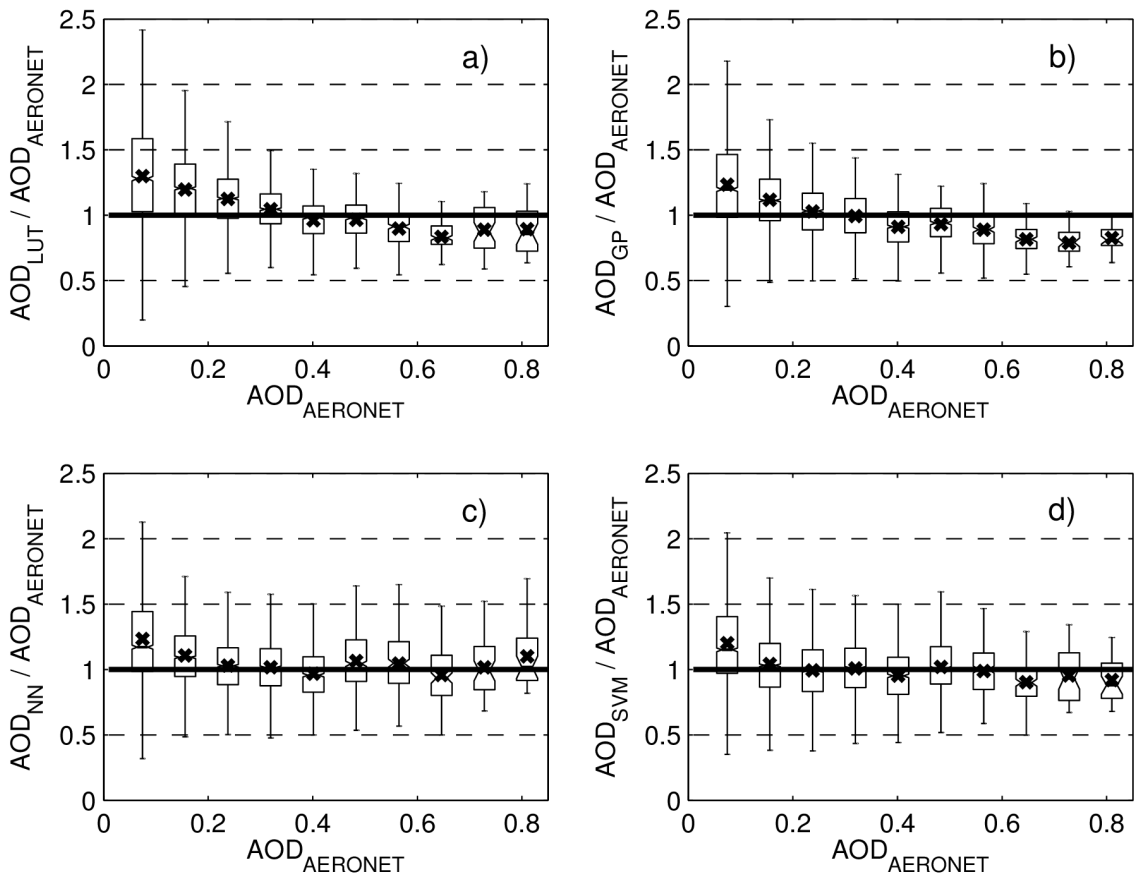
525

526

527

528





530

531 Figure 3: The same as Fig. 2, but in the vertical axis is the ratio of the predicted to the observed  
 532 (AERONET) AOD.

533

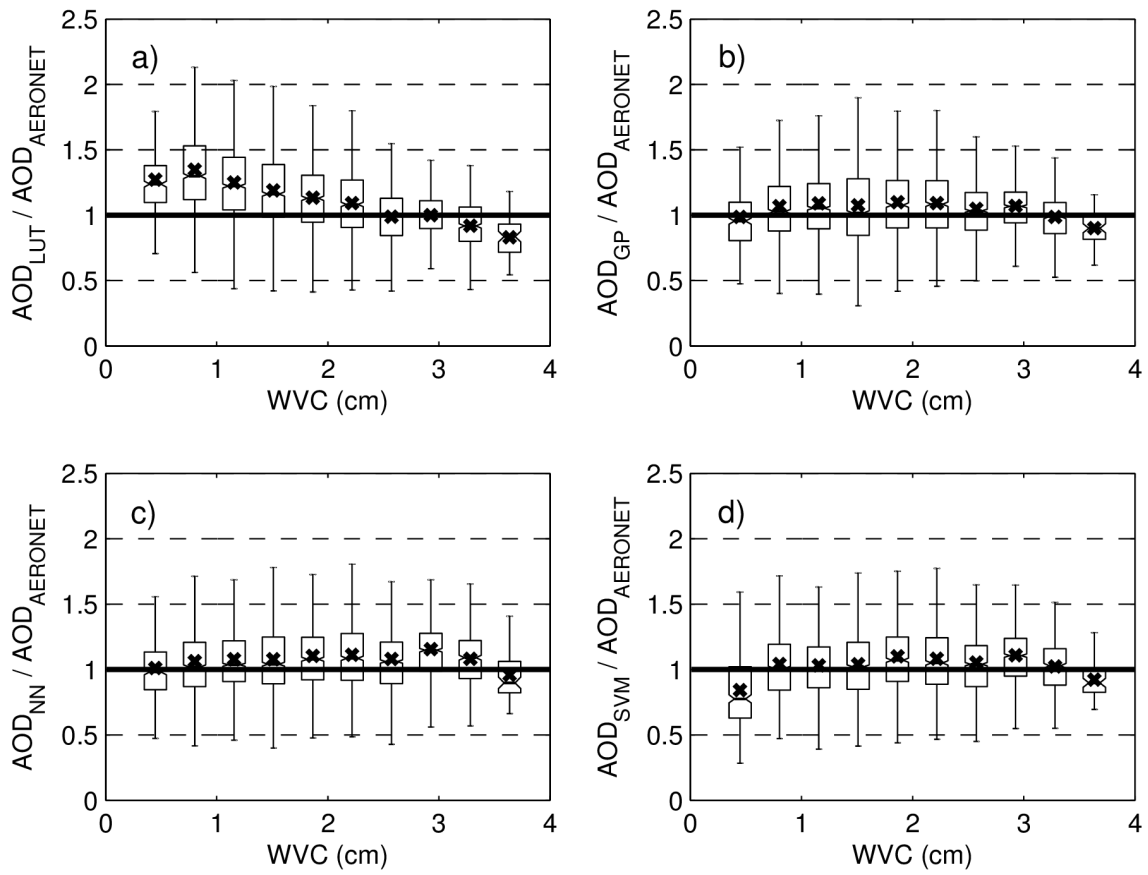
534

535

536

537

538



540

541 Figure 4: The same as Fig. 3, but the ratio of predicted to measured AOD is given as a function of the  
 542 water vapor column (WVC).

543

544

545

546

547

548

549

550

551

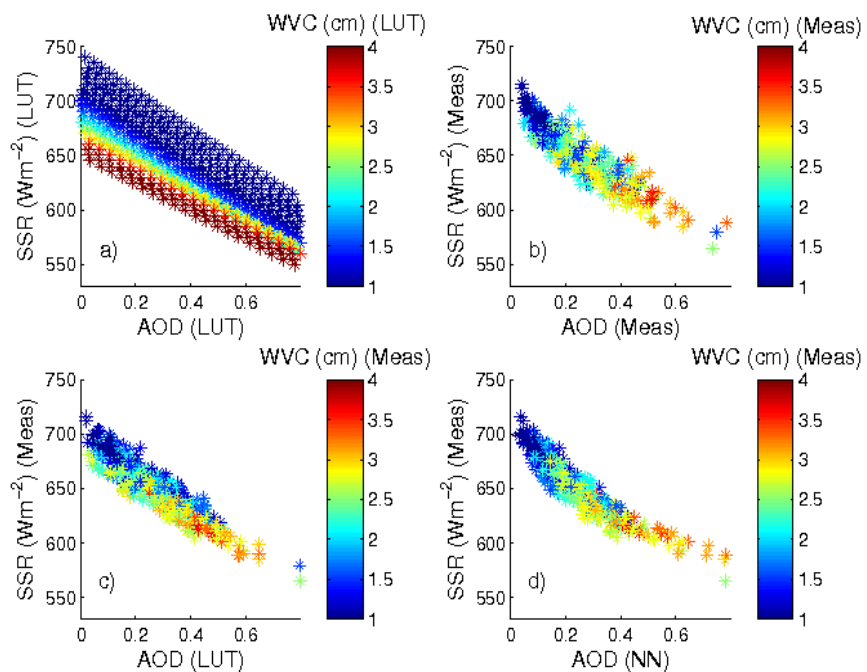
552

553

554

555

556



557

558

559

560

561

562

563 Figure 5: Solar surface radiation (SSR), aerosol optical depth (AOD) and water vapor column (WVC)

564 for a fixed solar zenith angle ( $48.50^{\circ}$ - $51.50^{\circ}$ ) for a) look-up table (LUT) and b) measurements (Meas).

565 The predicted AODs for c) LUT and d) neural network (NN) corresponding the same SSR, WVC and

566 SZA.

567

568

569

570

571

572

573

574

575

576

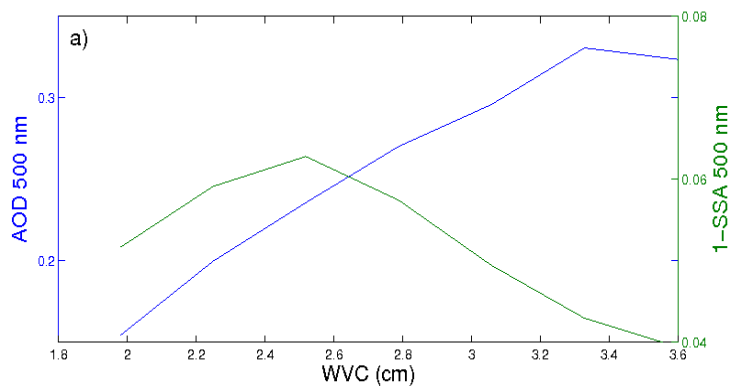
577

578

579

580

581



582

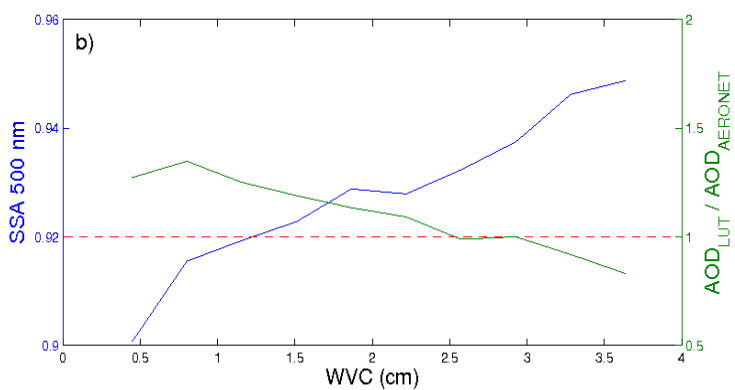
583

584

585

586

587



588 Figure 6: a) Aerosol optical depth (AOD), water vapor column (WVC) and 1-SSA at 500 nm from the

589 AERONET inversion sky data. b) SSA at 500 nm, WVC and the LUT's predicted AOD divided with the

590 observational AOD (AERONET), with the red line fixed to SSA (500 nm) = 0.92 (as in LUT).

591

592

593

594

595 **Appendix A**

596

597 Table A1. The statistics between the training and the validation data for the input and the output  
 598 parameters. The units for SZA, SSR and WVC are degrees,  $Wm^{-2}$  and cm, respectively.

Training:					
Parameter	Max	Min	Average	STD	Median
SZA	78.6	17.5	56.2	15.7	60.0
SSR	1071.9	120.5	522.7	247.1	479.6
WVC	4.12	0.23	2.23	0.73	2.29
AOD	1.06	0.01	0.22	0.12	0.20
Validation:					
Parameter	Max	Min	Average	STD	Median
SZA	78.7	17.5	60.6	14.7	65.3
SSR	1060.0	113.2	450.2	235.9	384.5
WVC	3.81	0.27	1.87	0.82	1.79
AOD	0.85	0.03	0.24	0.15	0.21

599

600 Table A2. The coefficient values of eq.(1) and errors (STD) for the NR method.

Coefficients	Estimate	STD error
$b_0$	$1.716 \times 10^5$	$8.372 \times 10^2$
$b_1$	$-1.696 \times 10^5$	$8.272 \times 10^2$
$b_2$	$-1.715 \times 10^5$	$8.363 \times 10^2$
$b_3$	$-1.206 \times 10^1$	$5.727 \times 10^{-1}$
$b_4$	$1.694 \times 10^5$	$8.264 \times 10^2$
$b_5$	$5.145 \times 10^0$	$2.465 \times 10^{-1}$
$b_6$	$6.819 \times 10^0$	$3.728 \times 10^{-1}$

601